nature materials

ARTICLES

https://doi.org/10.1038/s41563-022-01361-8

Designed growth of large bilayer graphene with arbitrary twist angles

Can Liu[1,2,12]✉, Zehui Li[1,12], Ruixi Qiao[3,4,12], Qinghe Wang[1,12], Zhibin Zhang[1], Fang Liu[1], Ziqi Zhou[1], Nianze Shang[1], Hongwei Fang[5], Meixiao Wang[5], Zhongkai Liu[5], Zuo Feng[1], Yang Cheng[1], Heng Wu[6], Dewei Gong[1], Song Liu[7], Zhensheng Zhang[7], Dingxin Zou[7], Ying Fu[8], Jun He[9], Hao Hong[1], Muhong Wu[3,10], Peng Gao[3], Ping-Heng Tan[6], Xinqiang Wang[1], Dapeng Yu[7], Enge Wang[3,8,11], Zhu-Jun Wang[5]✉ and Kaihui Liu[1,3]✉

The production of large-area twisted bilayer graphene (TBG) with controllable angles is a prerequisite for proceeding with its massive applications. However, most of the prevailing strategies to fabricate twisted bilayers face great challenges, where the transfer methods are easily stuck by interfacial contamination, and direct growth methods lack the flexibility in twist-angle design. Here we develop an effective strategy to grow centimetre-scale TBG with arbitrary twist angles (accuracy, <1.0°). The success in accurate angle control is realized by an angle replication from two prerotated single-crystal Cu(111) foils to form a Cu/TBG/Cu sandwich structure, from which the TBG can be isolated by a custom-developed equipotential surface etching process. The accuracy and consistency of the twist angles are unambiguously illustrated by comprehensive characterization techniques, namely, optical spectroscopy, electron microscopy, photoemission spectroscopy and photocurrent spectroscopy. Our work opens an accessible avenue for the designed growth of large-scale two-dimensional twisted bilayers and thus lays the material foundation for the future applications of twistronics at the integration level.

The advent of twist angle between bilayer graphene unambiguously provides an effective platform to engineer the band structure of graphene and hence its electronic and optical properties. By precisely adjusting the twist angles, exotic phenomena can be stimulated, such as the tunable Van Hove singularities[1–3], quantized anomalous Hall effect[4–6], unconventional superconductivity[7–9] and topological insulator states[10–12], which initiate the field of twistronics. To fully explore these emerging properties and accelerate their potential applications, the scalable growth of twisted bilayers with controllable angles and clean interfaces is desperately demanded.

To date, many efforts have been devoted to the fabrication of twisted bilayers, whose core idea is to couple two individual layers into a bilayer. These approaches can be roughly divided into two types, including the transfer methods, for example, polymer-based dry transfer[13,14] or liquid-assisted wet transfer[15,16], and folding methods, for example, by ultrasonic excitation[17], 'self-folding'[18] or through a micromanipulation technique such as scanning probe microscopy[19–21]. However, all these strategies are based on a post-production process, which suffers from issues of low throughput, harsh controllability or unavoidable interlayer contamination.

In fact, the most straightforward way to obtain large twisted bilayer graphene (TBG) with clean interfaces is to directly grow bilayers with a designed angle. Continuous efforts and progress have been made along this direction, for example, the hetero-site nucleation strategy[22], the atomic-stepped copper (Cu) arrangement technique[23] or the plasma-assistant growth process[24]. Specifically, 30° TBG can be frequently obtained since it has a lower formation energy compared with other twist angles around it[25,26]. However, the direct growth of bilayer graphene with arbitrarily designed twist angles has not been realized yet. The great challenges mainly include the following two aspects: (1) the two graphene layers tend to align parallelly since they experience the same surface topography of the epitaxial substrate, thereby forming energy-favourable AB-stacked bilayers[27–30]; (2) the direct nucleation of twisted bilayers only occurs randomly at the defect sites, tortuous steps or structured surfaces, where neither the twist angle nor the number of layers can be accurately controlled[25,31,32]. In light of the drawbacks in both post-stacking/folding methods and direct growth methods, it is in great demand to exploit new methods to acquire large bilayer graphene with designed twist angles.

Fortunately, unidirectional monolayer graphene can be unambiguously grown by surface-periodic-potential-guided epitaxial growth[33–37], where the direction of monolayer graphene is uniquely determined by the surface lattice orientation of the epitaxial substrate. Therefore, if two prestacked substrates are rotated with a

[1]State Key Laboratory for Mesoscopic Physics, Frontiers Science Center for Nano-optoelectronics, School of Physics, Peking University, Beijing, China. [2]Department of Physics, Renmin University of China, Beijing, China. [3]International Centre for Quantum Materials, Collaborative Innovation Centre of Quantum Matter, Peking University, Beijing, China. [4]Institute for Frontier Science, Nanjing University of Aeronautics and Astronautics, Nanjing, China. [5]ShanghaiTech Laboratory for Topological Physics, School of Physical Science and Technology, Shanghai Tech University, Shanghai, China. [6]State Key Laboratory of Superlattices and Microstructures, Institute of Semiconductors, Chinese Academy of Sciences, Beijing, China. [7]Shenzhen Institute for Quantum Science and Engineering, Southern University of Science and Technology, Shenzhen, China. [8]Songshan Lake Materials Laboratory, Institute of Physics, Chinese Academy of Sciences, Dongguan, China. [9]Key Laboratory of Artificial Micro- and Nano-structures of Ministry of Education, School of Physics and Technology, Wuhan University, Wuhan, China. [10]Interdisciplinary Institute of Light-Element Quantum Materials and Research Center for Light-Element Advanced Materials, Peking University, Beijing, China. [11]School of Physics, Liaoning University, Shenyang, China. [12]These authors contributed equally: Can Liu, Zehui Li, Ruixi Qiao, Qinghe Wang. ✉e-mail: canliu@pku.edu.cn; wangzhj3@shanghaitech.edu.cn; khliu@pku.edu.cn

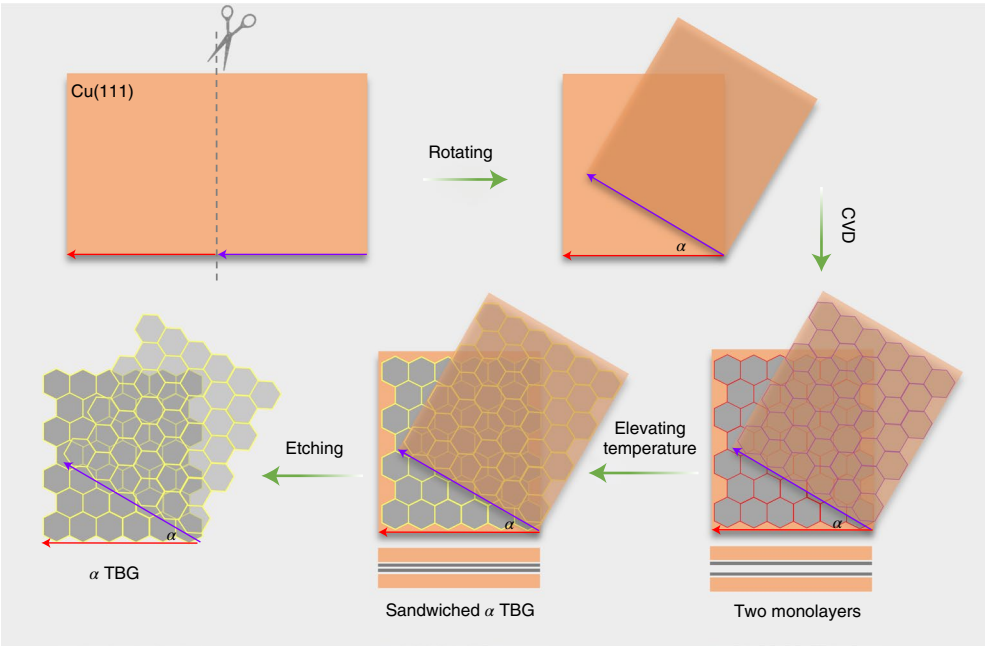

Fig. 1 | Schematic for the growth design of TBG. A piece of single-crystal Cu(111) foil was cut into two pieces with parallel edges (marked in red and violet). Then, the two pieces were stacked with rotation angle α between the two marked edges. After that, graphene was epitaxially grown between the two adjacent Cu(111) surfaces by the CVD method. Bilayer graphene with twist angle α was subsequently obtained by heating the Cu to an elevated temperature and was finally isolated after etching the Cu away.

designed twist angle, the epitaxially grown monolayers between the two substrates will inherently form a twisted structure, whose angle is accurately determined by the two rotated substrates. Based on this idea, we develop a strategy to grow bilayer graphene with a controllable twist angle by prerotating two single-crystal Cu(111) substrates. Different from the post-stacking/folding methods, the angle replication from the prestacked substrates can produce a clean interface and form an intrinsic van der Waals (vdW) coupled twisted bilayer. Additionally, in contrast to conventional growth methods, the twist angle is locked by the two Cu foils (Cu–graphene interaction of ~46 meV per atom (ref. [38]) is stronger than graphene–graphene vdW interaction of ~30 meV per atom (ref. [39])), and wide-range twist angles (even a small angle like 1°) could be achieved in principle. Therefore, this work provides an effective avenue for the precise design and massive fabrication of large TBG.

Strategy to produce TBG by angle replication

Single-crystal Cu(111) foil has been proven to be an ideal epitaxial substrate for graphene growth due to their surface symmetry matching (both have C_3 rotational symmetry) and small lattice mismatch (4%), which ensure the consistent orientation of graphene domains and further formation of large single-crystal graphene film[40]. In our design (Fig. 1), a single-crystal Cu(111) foil with a straight edge was chosen and then cut into two pieces. Since the edges of the two obtained pieces (Fig. 1, red and violet arrows) are parallel, the angle between the lattice orientations of the two Cu foils is equivalent to the rotation of the marked edges.

After stacking the two pieces and fixing them with a designed rotation angle α, graphene was epitaxially grown on the single-crystal Cu(111) surfaces by the chemical vapour deposition (CVD) method. Two monolayer graphene films were formed between adjacent Cu foils, and therefore, the rotation angle α was replicated from the Cu foils due to the fixed orientation in epitaxial growth. Subsequently, the temperature was further elevated to ensure the soft Cu foil and flat Cu surface (Supplementary Fig. 1), where the graphene–graphene vdW interaction themselves lead to the formation of a uniform bilayer with a replicated rotation angle α. Finally, to peel the TBG off, an equipotential surface etching method was developed to homogeneously remove the Cu foil on one side. Through this strategy, we can obtain large bilayer graphene with arbitrary twist angles by artificially replicating the relative rotation angle of Cu foils on a macroscale.

Confirmation of angle replication

High-quality single-crystal Cu foil with the (111) facet index was obtained through the seeded growth method[41] (Methods and Supplementary Fig. 2a) and was further electropolished to access a smoother surface with a roughness within 20 nm (ref. [42]). Electron backscatter diffraction (EBSD) and X-ray diffraction (XRD) were employed to verify the single-crystalline nature of the Cu foil. Both large-area uniform blue colour in the inverse pole figure (IPF) maps (Fig. 2b and Supplementary Fig. 2c–e) and the pronounced Cu(111) peak in the XRD 2θ-scan data (Supplementary Fig. 2b) verify the high-quality (111) facet of the as-prepared Cu foil. Here the application of high-quality single-crystal Cu(111) substrates is the basis for ensuring the highly orientated single-crystal graphene domains.

Following the strategy indicated in Fig. 1, two Cu foils derived from the same single-crystal Cu(111) were stacked with a designed rotation angle α (here we choose $\alpha = 14°$ as an example; Methods and Supplementary Fig. 3). To accurately measure the rotation angle between the two Cu(111) foils (noted as 1 and 2; Fig. 2a), the EBSD pole figures (PFs) were collected on Cu(111)-1 and Cu(111)-2, which present a relative rotation angle of 14.3° (Fig. 2c). In the XRD φ-scan data, the three-fold symmetry of the diffraction peaks corresponding to Cu(002) indicates the high crystallinity of Cu(111) and gives a relative rotation angle of 14.2° between the two Cu foils (Fig. 2d). Using these two methods, nine samples (with the designed angle of $\alpha = 14°$) were measured to evaluate the manual operation deviations. Both EBSD (Fig. 2e) and XRD (Supplementary Fig. 4) statistical data showed that all the rotation angles are distributed

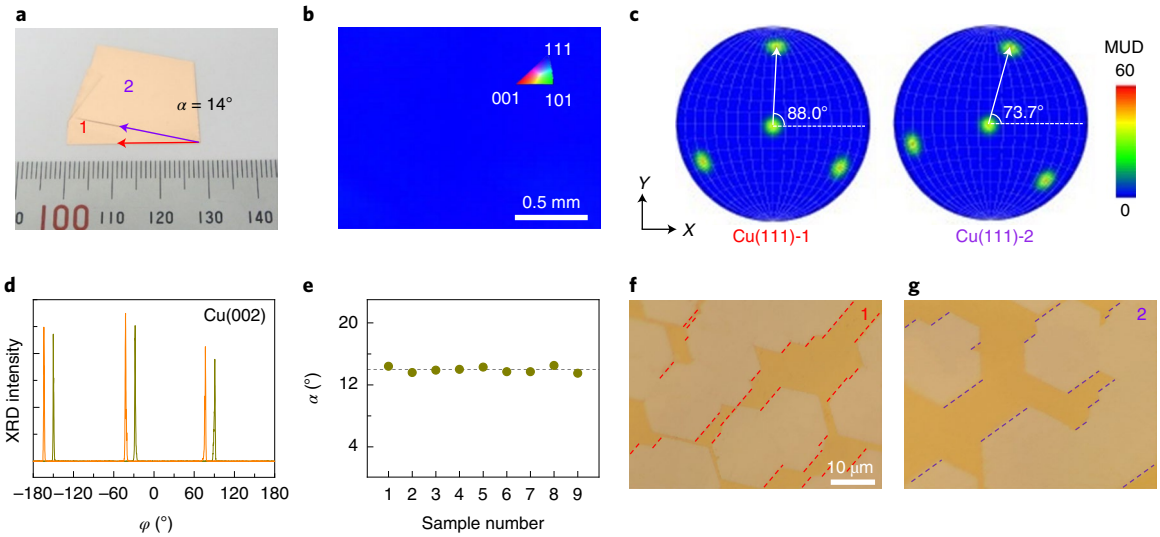

Fig. 2 | Twist-angle replication from the rotated Cu foils. a, Photograph of two stacked Cu foils with rotation angle α. The numbers on the ruler indicate the length in millimetres. **b**, EBSD IPF map of the Cu foil. The uniform blue colour reveals the single-crystal structure of the (111) facet index. **c**, EBSD PFs of the two Cu pieces, marked as Cu(111)-1 and Cu(111)-2. The multiples of uniform density (MUD) results present a relative rotation angle of 14.3°. **d**, XRD φ-scan data for Cu(111)-1 (orange curve) and Cu(111)-2 (dark yellow curve) obtained by fixing along the Cu(002) direction. The three-fold symmetry of diffraction peaks indicates the high crystallinity and a shift of 14.2° between the two spectra. **e**, Statistical data of the rotation angles for nine stacked Cu foils measured by EBSD, indicating the small deviation of ~1.0°. **f**,**g**, Optical images of the hexagonal graphene domains on the top surfaces of Cu(111)-1 (**f**) and Cu(111)-2 (**g**), with a relative rotation angle of ~14°.

between 13.5° and 14.5°, indicating that the experimental accuracy of the rotation angle control for Cu foils is within 1.0°.

Furthermore, to check the replication effect of the twist angles, individual graphene domains were epitaxially grown simultaneously on the two Cu foils. Aligned hexagonal domains are observed on the surface of each Cu(111) substrate, and the relative angle of graphene between the two Cu foils is ~14°, which is consistent with the designed angle of Cu stacking (Fig. 2f,g). To realize the full coverage of graphene monolayers between the two Cu foils, the epitaxial growth of graphene was accomplished at 1,050 °C (Methods). In the following procedure, we raised the temperature to ~1,074 °C, at which the Cu foils become soft and their surfaces are atomically flat. Then, the graphene–graphene vdW interaction leads to the automatic formation of Cu/TBG/Cu sandwich structure with an intrinsically clean interface between the two graphene layers (Supplementary Fig. 5). The control of this elevated temperature is critical to form high-quality bilayers. If it is too low, for example, 1,060 °C, the two graphene/Cu layers cannot be adhered seamlessly, resulting in an ~20 μm gap between them. If it is too high, for example, 1,080 °C, the Cu foils can be easily melted (Supplementary Fig. 6).

Equipotential surface etching method to isolate bilayer graphene

Bilayer graphene was successfully isolated from the sandwich structure via a custom-developed equipotential surface etching method to remove the Cu foil on one side (Fig. 3a). Here two parallel Pt electrodes were immersed into an $(NH_4)_2S_2O_8$ solution to establish a uniform electric field. The Cu/TBG/Cu sandwich structure with one side protected by a thermal release tape (TRT) was parallel to the two electrodes in the solution, ensuring an equipotential surface on the Cu foil. During the etching process, Cu^{2+} ions equably dissolved from the surface of the Cu foil and migrated along the direction of electric field, and finally deposited on the cathode, instead of gathering near the surface of the Cu foil or forming a complex with $S_2O_8^{2-}$, thereby avoiding heterogeneous etching and decrease in etching speed[43].

Meanwhile, to monitor the accurate time of graphene exposure, the amperometric method was applied to track the etching degree (Methods). As shown in Fig. 3b, the current slightly decreases before approaching the surface of bilayer graphene due to the reduction in roughness and thickness of the Cu foil during equable etching. When close to the graphene layers, a significant concave current change occurs, attributable to the inert electrochemistry of exposed graphene[44] and the increased specific surface area of the etched Cu foil on the other side[45,46]. Experimentally, once the trend of concave current appears, the complete bilayer graphene can be extracted in the next ~6 min (Fig. 3b (inset) and Supplementary Fig. 7), with a representative area of ~2 cm × 1 cm (Fig. 3c).

Subsequently, the centimetre-scale bilayer film was transferred onto the SiO_2/Si substrate by a commonly used wet transfer method (Methods). The uniform contrast in the optical images demonstrates the full coverage of bilayer graphene (Fig. 3d and Supplementary Fig. 8). The Raman mappings of the 2D/G intensity ratio (I_{2D}/I_G) and R-mode intensity prove the uniformity of the fabricated ~14° TBG (Fig. 3e,f and Supplementary Fig. 9). In addition, the appearance of the layer-breathing mode in the Raman spectra demonstrates the well-coupled characteristic between the two layers (Supplementary Fig. 10). The twist angle of ~14° was further confirmed by the moiré pattern in the high-resolution transmission electron microscopy (HRTEM) images and the corresponding fast Fourier transform image (Fig. 3g and Supplementary Fig. 11). Meanwhile, the statistical results extracted by 140 selected area electron diffraction (SAED) patterns of a millimetre-scale 14° TBG showed a narrow distribution of twist angles of approximately 1.0° (Supplementary Fig. 12), which is consistent with our design. Angle-resolved photoemission spectroscopy (ARPES) unequivocally revealed the typical band dispersion of the twisted bilayer (Fig. 3h,i). The constant-energy contours at different binding energies showed that two Dirac cones shifted in momentum space due to the twist angle of ~14°, where the top layer (left) had higher intensity and the bottom layer (right) had lower intensity (because of matrix element effects, only the part of the band corresponding to $k > K$ ($K \approx 1.70$ Å^{-1}) is visible)[47].

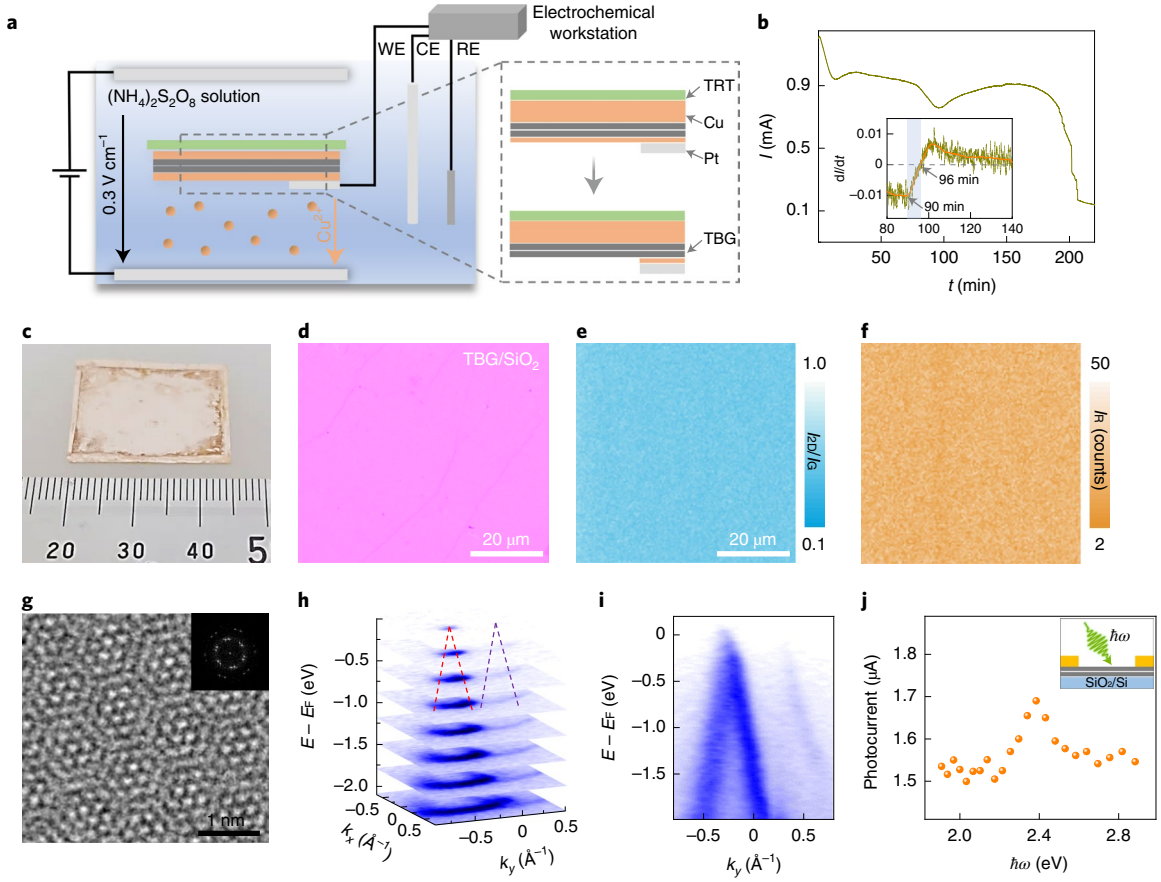

Fig. 3 | Characterizations of TBG. a, Schematic of the equipotential surface etching process. TBG was obtained by etching one side of the Cu(111) foil with the other side protected by TRT. The three-electrode system consists of a working electrode (WE), reference electrode (RE) and counter electrode (CE). **b**, Time (t) evolution of current (I) during the etching process. The inset shows the time evolution of the derivative of current during the etching process. **c**, Photograph of the Cu(111) foil with a freshly exposed bilayer graphene film. The numbers on the ruler indicate the length in millimetres. **d**, Optical image of bilayer graphene after transferring onto the SiO_2/Si substrate. **e**,**f**, Raman mappings of I_{2D}/I_G and I_R, verifying the uniformity of the obtained bilayer graphene film. **g**, HRTEM image of bilayer graphene. The inset shows the fast Fourier transform pattern of the HRTEM image. **h**, Stacking plot of constant-energy contours at different binding energies in k_x–k_y plane of the bilayer graphene. **i**, ARPES spectrum of the bilayer graphene across the two adjacent Dirac cones of **h** along the k_y direction. **j**, Photocurrent versus the photon energy ($\hbar\omega$) of incident light. These results prove that the twist angle of bilayer graphene is ~14°.

The photocurrent data of twisted-bilayer-based devices (Fig. 3j and Supplementary Fig. 13) exhibited the same peak positions at ~520 nm (photon energy, 2.38 eV), which is consistent with the transition energy between the two Van Hove singularities of 14° TBG (ref. [48]).

Tunability of twist angles

Our growth method is proven to be applicable to various twist angles by facilely controlling the stacking angles of Cu foils. Raman spectroscopy was used to characterize bilayer graphene since it possesses rich vibrational signatures compared with monolayers[49,50], such as the varied intensity ratio of I_{2D}/I_G and the full-width at half-maximum (FWHM) of the 2D band, as well as the rotation-induced intra- and intervalley scattering modes of R′ and R band at small twist angles ($3° < \theta < 9°$) and near the critical angle ($\theta_c \approx 12°$), respectively.

Here we deliberately chose the designed rotation angle α as 0°, 5°, 12° and 30° at which apparent variations were observed in their Raman spectra (Fig. 4a–d). For the parallelly stacked Cu foils ($\alpha = 0°$), the I_{2D}/I_G ratio and the FWHM of the 2D band are indicated to be ~1.2 and ~57 cm^{-1}, respectively (Fig. 4a), which are typical characteristics of AB-stacked bilayer graphene. In addition, the corresponding moiré pattern in the HRTEM image and SAED pattern also confirm the AB-stacking order (Fig. 4e,i), where the intensity ratio between the diffraction spots $(11\bar{2}0)$ and $(10\bar{1}0)$ is greater than 2. This phenomenon can be well understood since the AB-stacked structure is the most stable one with a twist angle of 0° (refs. [51,52]).

For the $\alpha = 5°$ case, the absence of the defect-induced peaks of the D (~1,350 cm^{-1}) and D′ (~1,620 cm^{-1}) bands manifests the emerging peak as the R′ band at the position of ~1,622 cm^{-1}. Meanwhile, the I_{2D}/I_G ratio and FWHM of the 2D band are ~1.0 and ~36 cm^{-1}, respectively (Fig. 4b). All these features suggest a small twist angle, which is finalized as ~5.3° by the HRTEM image and SAED pattern (Fig. 4f,j). When α is designed as 12°, a pronounced G-peak enhancement and a tiny R peak located at ~1,478 cm^{-1} are observed (Fig. 4c,g,k), which can be attributed to the resonant excitation photon energy with the energy separation of the Van Hove singularities. Moreover, bilayer graphene with a twist angle of 30° can also be accurately fabricated (Fig. 4h,l), whose I_{2D}/I_G ratio is ~4.4 and 2D-band FWHM is ~27 cm^{-1} (Fig. 4d). Large-area Raman mappings of the typical peaks further confirmed the small-angle deviation of the as-synthesized bilayer graphene (Supplementary Fig. 14).

Till now, the direct growth of bilayers with small twist angles is extremely challenging, as they will automatically tend to transform to the energy-minimum state with a twist angle of 0° at higher

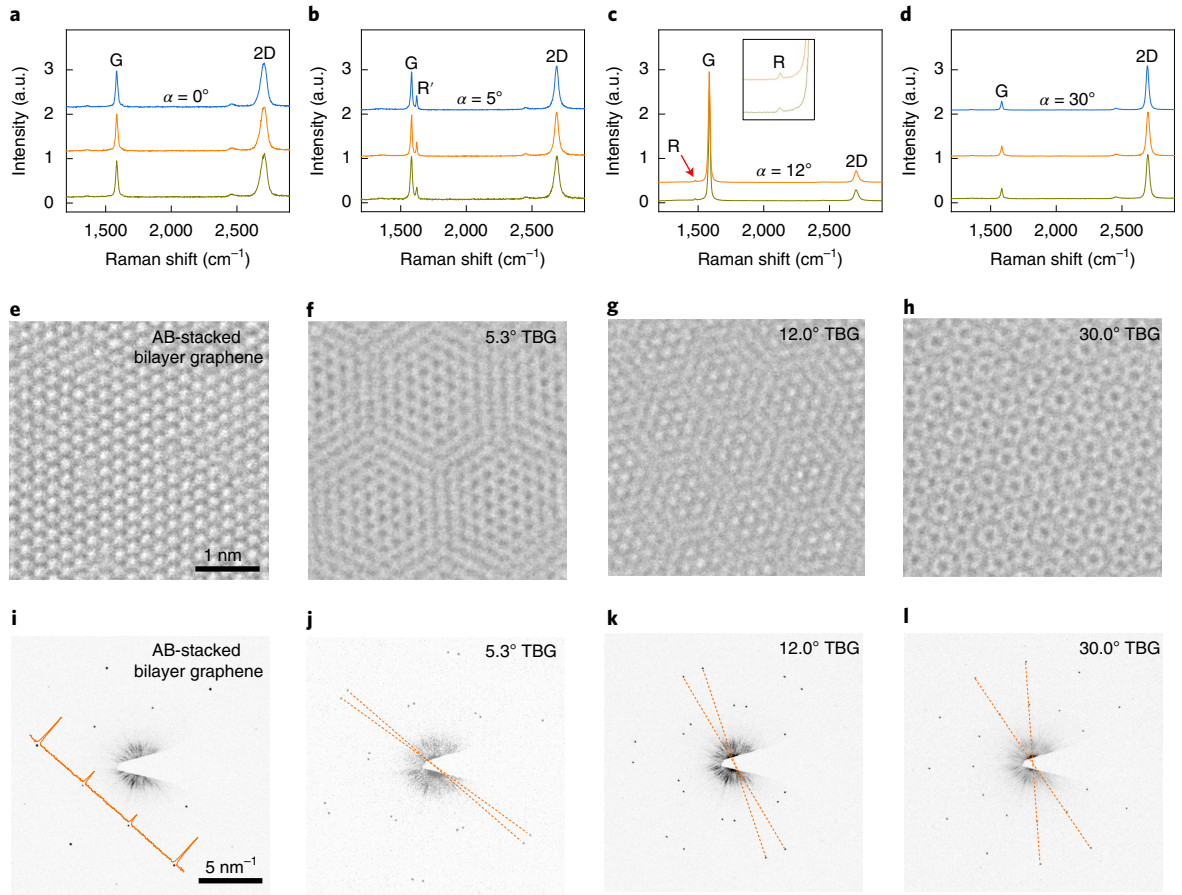

Fig. 4 | Angle tunability in TBG. a–**l**, Raman spectra (**a**–**d**), HRTEM images (**e**–**h**) and SAED patterns (**i**–**l**) of TBG with the designed twist angles α of 0°, 5°, 12° and 30°, respectively. The Raman spectra in different colours represent different positions, and each curve has been vertically shifted for clarity. The inset in **c** shows a zoomed-in view of the spectra of the R peak. The curve in **i** represents the intensity profile.

temperature[53,54]. In our design, the twist angle is locked by the two Cu foils and now make it possible to realize the small twist angles in CVD growth. We successfully grew bilayer graphene with a designed twist angle of 1° (Supplementary Fig. 15). The HRTEM image showed a clear moiré pattern with a period of ~15 nm, corresponding to a twist angle of ~0.94°. Furthermore, the SAED pattern indicated a twist angle of ~1° as well.

Conclusions

We report an angle replication strategy to produce large TBG, which can get rid of interfacial contamination between the two layers occurring in conventional methods. The twist angles of bilayer graphene can be readily tuned by predesigning the rotation angle of the two single-crystal Cu(111) foils, and an equipotential surface etching method is developed to isolate it from the Cu/TBG/Cu sandwich structure. The flexibility in arbitrary twist-angle design and the productivity in centimetre scale demonstrate the advances of our strategy. In view of the similar growth mechanism of two-dimensional materials, we propose that the way to tune the twist angles of bilayer graphene derived in this work can guide the growth of other twisted crystalline two-dimensional materials, thereby providing the material foundation for future device applications of twistronics.

Online content

Any methods, additional references, Nature Research reporting summaries, source data, extended data, supplementary information, acknowledgements, peer review information; details of author contributions and competing interests; and statements of data and code availability are available at https://doi.org/10.1038/s41563-022-01361-8.

Received: 10 May 2021; Accepted: 10 August 2022;
Published online: 15 September 2022

References

1. Li, G. et al. Observation of Van Hove singularities in twisted graphene layers. *Nat. Phys.* **6**, 109–113 (2009).
2. Yan, W. et al. Angle-dependent Van Hove singularities in a slightly twisted graphene bilayer. *Phys. Rev. Lett.* **109**, 126801 (2012).
3. Brihuega, I. et al. Unraveling the intrinsic and robust nature of Van Hove singularities in twisted bilayer graphene by scanning tunneling microscopy and theoretical analysis. *Phys. Rev. Lett.* **109**, 196802 (2012).
4. Zhang, Y.-H. et al. Nearly flat Chern bands in moiré superlattices. *Phys. Rev. B* **99**, 075127 (2019).
5. Sharpe, A. L. et al. Emergent ferromagnetism near three-quarters filling in twisted bilayer graphene. *Science* **365**, 605–608 (2019).
6. Serlin, M. et al. Intrinsic quantized anomalous Hall effect in a moiré heterostructure. *Science* **367**, 900–903 (2020).
7. Cao, Y. et al. Unconventional superconductivity in magic-angle graphene superlattices. *Nature* **556**, 43–50 (2018).
8. Yankowitz, M. et al. Tuning superconductivity in twisted bilayer graphene. *Science* **363**, 1059–1064 (2019).
9. Roy, B. & Juričić, V. Unconventional superconductivity in nearly flat bands in twisted bilayer graphene. *Phys. Rev. B* **99**, 121407 (2019).
10. Cao, Y. et al. Correlated insulator behaviour at half-filling in magic-angle graphene superlattices. *Nature* **556**, 80–84 (2018).
11. Lu, X. et al. Superconductors, orbital magnets and correlated states in magic-angle bilayer graphene. *Nature* **574**, 653–657 (2019).
12. Codecido, E. et al. Correlated insulating and superconducting states in twisted bilayer graphene below the magic angle. *Sci. Adv.* **5**, eaaw9770 (2019).

13. Castellanos-Gomez, A. et al. Deterministic transfer of two-dimensional materials by all-dry viscoelastic stamping. *2D Mater.* **1**, 011002 (2014).
14. Pizzocchero, F. et al. The hot pick-up technique for batch assembly of van der Waals heterostructures. *Nat. Commun.* **7**, 11894 (2016).
15. Robinson, J. T. et al. Electronic hybridization of large-area stacked graphene films. *ACS Nano* **7**, 637–644 (2013).
16. Nguyen, V. L. et al. Wafer-scale single-crystalline AB-stacked bilayer graphene. *Adv. Mater.* **28**, 8177–8183 (2016).
17. Zhang, J. et al. Free folding of suspended graphene sheets by random mechanical stimulation. *Phys. Rev. Lett.* **104**, 166805 (2010).
18. Wang, B. et al. Controlled folding of single crystal graphene. *Nano Lett.* **17**, 1467–1473 (2017).
19. Carozo, V. et al. Resonance effects on the Raman spectra of graphene superlattices. *Phys. Rev. B* **88**, 085401 (2013).
20. Ribeiro-Palau, R. et al. Twistable electronics with dynamically rotatable heterostructures. *Science* **361**, 690–693 (2018).
21. Chen, H. et al. Atomically precise, custom-design origami graphene nanostructures. *Science* **365**, 1036–1040 (2019).
22. Sun, L. et al. Hetero-site nucleation for growing twisted bilayer graphene with a wide range of twist angles. *Nat. Commun.* **12**, 2391 (2021).
23. Cho, H. et al. Specific stacking angles of bilayer graphene grown on atomic-flat and -stepped Cu surfaces. *npj 2D Mater. Appl.* **4**, 35 (2020).
24. Chen, Y.-C. et al. Direct growth of mm-size twisted bilayer graphene by plasma-enhanced chemical vapor deposition. *Carbon* **156**, 212–224 (2020).
25. Yan, Z. et al. Large hexagonal bi- and trilayer graphene single crystals with varied interlayer rotations. *Angew. Chem. Int. Ed.* **53**, 1565–1569 (2014).
26. Pezzini, S. et al. 30°-twisted bilayer graphene quasicrystals from chemical vapor deposition. *Nano Lett.* **20**, 3313–3319 (2020).
27. Zhou, H. et al. Chemical vapour deposition growth of large single crystals of monolayer and bilayer graphene. *Nat. Commun.* **4**, 2096 (2013).
28. Ma, W. et al. Interlayer epitaxy of wafer-scale high-quality uniform AB-stacked bilayer graphene films on liquid Pt_3Si/solid Pt. *Nat. Commun.* **10**, 2809 (2019).
29. Huang, M. et al. Large-area single-crystal AB-bilayer and ABA-trilayer graphene grown on a Cu/Ni(111) foil. *Nat. Nanotechnol.* **15**, 289–295 (2020).
30. Nguyen, V. L. et al. Layer-controlled single-crystalline graphene film with stacking order via Cu–Si alloy formation. *Nat. Nanotechnol.* **15**, 861–867 (2020).
31. Brown, L. et al. Twinning and twisting of tri- and bilayer graphene. *Nano Lett.* **12**, 1609–1615 (2012).
32. Chu, C. M. & Woon, W. Y. Growth of twisted bilayer graphene through two-stage chemical vapor deposition. *Nanotechnology* **31**, 435603 (2020).
33. Lee, J.-H. et al. Wafer-scale growth of single-crystal monolayer graphene on reusable hydrogen-terminated germanium. *Science* **344**, 286–289 (2014).
34. Xu, X. et al. Ultrafast epitaxial growth of metre-sized single-crystal graphene on industrial Cu foil. *Sci. Bull.* **62**, 1074–1080 (2017).
35. Deng, B. et al. Wrinkle-free single-crystal graphene wafer grown on strain-engineered substrates. *ACS Nano* **11**, 12337–12345 (2017).
36. Zhang, X. et al. Epitaxial growth of 6 in. single-crystalline graphene on a Cu/Ni (111) film at 750 °C via chemical vapor deposition. *Small* **15**, 1805395 (2019).
37. Liu, C., Wang, L., Qi, J. & Liu, K. Designed growth of large-size 2D single crystals. *Adv. Mater.* **32**, 2000046 (2020).
38. Hamada, I. & Otani, M. Comparative van der Waals density-functional study of graphene on metal surfaces. *Phys. Rev. B* **82**, 153412 (2010).
39. Liu, Z. et al. Interlayer binding energy of graphite: a mesoscopic determination from deformation. *Phys. Rev. B* **85**, 205418 (2012).
40. Nguyen, V. L. et al. Seamless stitching of graphene domains on polished copper (111) foil. *Adv. Mater.* **27**, 1376–1382 (2015).
41. Wu, M. et al. Seeded growth of large single-crystal copper foils with high-index facets. *Nature* **581**, 406–410 (2020).
42. Griep, M. H., Sandoz-Rosado, E., Tumlin, T. M. & Wetzel, E. Enhanced graphene mechanical properties through ultrasmooth copper growth substrates. *Nano Lett.* **16**, 1657–1662 (2016).
43. Zhang, X. et al. High-quality graphene transfer via directional etching of metal substrates. *Nanoscale* **11**, 16001–16006 (2019).
44. Yang, X. et al. Clean and efficient transfer of CVD-grown graphene by electrochemical etching of metal substrate. *J. Electroanal. Chem.* **688**, 243–248 (2013).
45. Cui, C., Lim, A. T. O. & Huang, J. A cautionary note on graphene anti-corrosion coatings. *Nat. Nanotechnol.* **12**, 834–835 (2017).
46. Wu, L. et al. Effects of normal load and etching time on current evolution of scratched GaAs surface during selective etching. *Mater. Sci. Semicond. Process.* **105**, 104744 (2020).
47. Forti, S. et al. Mini-Dirac cones in the band structure of a copper intercalated epitaxial graphene superlattice. *2D Mater.* **3**, 035003 (2016).
48. Havener, R. W. et al. Van Hove singularities and excitonic effects in the optical conductivity of twisted bilayer graphene. *Nano Lett.* **14**, 3353–3357 (2014).
49. Wu, J. B. et al. Resonant Raman spectroscopy of twisted multilayer graphene. *Nat. Commun.* **5**, 5309 (2014).
50. Chen, G. et al. Tunable correlated Chern insulator and ferromagnetism in a moiré superlattice. *Nature* **579**, 56–61 (2020).
51. Alden, J. S. et al. Strain solitons and topological defects in bilayer graphene. *Proc. Natl Acad. Sci. USA* **110**, 11256–11260 (2013).
52. Hong, H. et al. Interfacial engineering of van der Waals coupled 2D layered materials. *Adv. Mater. Interfaces* **4**, 1601054 (2017).
53. Shibuta, Y. & Elliott, J. A. Interaction between two graphene sheets with a turbostratic orientational relationship. *Chem. Phys. Lett.* **512**, 146–150 (2011).
54. Wang, D. et al. Thermally induced graphene rotation on hexagonal boron nitride. *Phys. Rev. Lett.* **116**, 126101 (2016).

Methods

Production of single-crystal Cu(111). A piece of polycrystalline Cu foil (25 μm thick, 99.8%, Sichuan Oriental Stars Trading, #Cu-1031) was placed on a flat quartz substrate and then loaded into a hot-wall tube furnace (Tianjin Kaiheng, custom designed). The furnace was ramped to 1,020 °C in 1 h and maintained at this temperature for 2 h under 500 s.c.c.m. Ar and 50 s.c.c.m. H_2. The reduced atmosphere is necessary for both heating and annealing processes to obtain single-crystal Cu(111).

Procedure for designing prerotated Cu foils. A commercialized two-dimensional-material rotary transfer stage (JOOIN Technology, 2DT-7-300) was used to realize the rotating and stacking of single-crystal Cu(111) foils. The instrument has a rotation resolution of 0.1° and an in-plane displacement resolution of 3 μm. Specific operation steps are shown as below. (1) Divide a single-crystal Cu(111) foil with a horizontal edge into two pieces and parallelly align them on the platform under an optical microscope. (2) Lift the top piece of the Cu foil by adhesive polydimethylsiloxane, and rotate the bottom Cu foil via the stage with designed angle α. Then, drop the top foil onto the bottom one and apply a slight pressure through the polydimethylsiloxane. (3) Fold the non-overlapping part of the bottom foil to fix the relative rotation angle, release the polydimethylsiloxane away from the top foil and then fold the non-overlapping part of the top Cu foil.

CVD growth of TBG. The prestacked smooth single-crystal Cu(111) foils with rotation angle α were placed on a quartz plate and loaded into the centre of a hot-wall tube furnace, which has a heating area of Φ60 mm × 400 mm (Hefei Kejing Materials Technology, OTF-1200X). Then, the system was flushed with Ar and heated to 1,050 °C under 500 s.c.c.m. Ar and 10 s.c.c.m. H_2. During growth, 1 s.c.c.m. of 1% CH_4 (diluted by Ar) was introduced as the carbon source for 6 h, and the furnace was heated to 1,074 °C for 30 min to form the bilayers. After that, the system was naturally cooled down to room temperature under 500 s.c.c.m. Ar and 10 s.c.c.m. H_2.

Equipotential surface etching of Cu. Graphene grown on the external surface of Cu foils was removed by air plasma. Then, one side of the Cu/TBG/Cu structure was pasted on the TRT, and polymethyl methacrylate (PMMA) was used to seal the edges of Cu foils to prevent the occurrence of etching along the edges. The sample was placed into 100 ml of 0.1 M $Na_2S_2O_8$ solution, and paralleled to the two Pt electrodes with a constant electric-field intensity of 0.3 V cm^{-1}. The exposed side of the Cu foil was uniformly etched under the equipotential electric field. A typical three-electrode system was applied to monitor the current change on the sample surface during the etching process, which can reflect the resistance change (including sample, interface and solution resistance) and indicate the appearance of graphene layers. The sample was fixed by the Pt electrode clamp and served as the working electrode. A saturated calomel electrode and platinized platinum electrode were used as the reference electrode and counter electrode, respectively. The constant potential is set as 0.05 V versus saturated calomel electrode.

Transfer of TBG. The obtained TBG was transferred onto SiO_2/Si or holey-carbon-film TEM grids by the PMMA-assisted method. The graphene film was spin coated with PMMA and baked at 120 °C for 3 min. Then, 4% $Na_2S_2O_8$ solution was used to etch the Cu away. After rinsing with deionized water, the PMMA/graphene film was transferred onto the SiO_2/Si or holey-carbon-film TEM grids. Subsequently, the PMMA was removed by acetone.

Characterizations of TBG. Optical images were taken by an Olympus BX51M microscope. The EBSD characterizations were performed using a PHI 710 Scanning Auger Nanoprobe instrument, and the IPF and PF maps were obtained from the Oxford Aztec software version 3.1. The XRD φ-scan measurements were carried out by a PANalytical X'Pert Pro system with a Cu target. The typical probing area is 1.2 cm × 0.5 cm. The XRD 2θ-scan measurements were conducted using a Bruker D8 Advance system with a Cu target. Raman spectra and mappings were collected by the custom-designed optical systems with the excitation wavelength of 514 nm. Low-frequency Raman spectra were collected by a Horiba HR800 system with the excitation wavelength of 532 nm. HRTEM/SAED experiments were performed using an FEI Titan Themis G2 300 instrument operated at 300 kV, and the size of the selected area aperture during the diffraction experiment was chosen to be ~200 nm. The ARPES measurements were performed at the nano ARPES beamline BL07U of the Shanghai Synchrotron Radiation Facility, China, with a beam spot size of ~500 nm and energy/momentum resolution of 50 meV per 0.2°. The data were collected by DA30L analysers at this facility. TBG was transferred onto the BN/SiO_2/Si substrate and measured in an ultrahigh vacuum with a base pressure of more than 5×10^{-11} mbar and photon energy of 91 eV.

Photoelectric device fabrication and measurement. The two-terminal devices were fabricated through micro-/nanoprocessing. Ti/Au electrodes were evaporated by electron-beam lithography on the TBG transferred onto the SiO_2/Si substrate. A supercontinuum light source (400–1,800 nm) combined with a laser-line-tunable optical filter was applied to generate a monochromatic laser beam (spot size, ~3 μm). The photocurrent was recorded by an electrochemical station when the laser was focused on the central region of the sample. During the detection, the laser power and applied voltage were kept constant at 80 μW and 0.25 V, respectively.

Data availability

Source data are provided with this paper. All other data that support the findings of this study are available within the Article and the Supplementary Information.

Acknowledgements

This work was supported by Guangdong Major Project of Basic and Applied Basic Research with grant no. 2021B0301030002 (E.W. and K.L.); Beijing Natural Science Foundation under grant no. JQ19004 (K.L.); the National Natural Science Foundation of China under grant nos. 52025023 (K.L.), 51991342 (K.L.), 52021006 (K.L.), 11888101 (E.W.), 92163206 (M. Wu), 12027804 (Z.-J.W.), 52172035 (M. Wu), 52100115 (Z. Li), 52125307 (P.G.) and T2188101 (K.L.); the National Key R&D Program of China under grant nos. 2021YFB3200303 (K.L.), 2021YFA1400201 (H.H.), 2021YFA1400502 (M. Wu) and 2018YFA0703700 (J.H.); the Key R&D Program of Guangdong Province under grant nos. 2020B010189001 (K.L.), 2019B010931001 (K.L.) and 2018B030327001 (D.Y.); the Strategic Priority Research Program of Chinese Academy of Sciences with grant no. XDB33000000 (K.L.); the Pearl River Talent Recruitment Program of Guangdong Province with grant no. 2019ZT08C321 (K.L.). We acknowledge the Electron Microscopy Laboratory in Peking University for use of the electron microscope.

Author contributions

K.L., Z.-J.W. and C.L. conceived the project. C.L., Z. Li and Q.W. performed the growth experiments. Z. Li and R.Q. conducted the equipotential surface etching experiments. Q.W., Z. Zhang, F.L. and X.W. performed the EBSD and XRD measurements. R.Q., P.G. and D.Y. performed the HRTEM and SAED experiments. C.L., Y.C., H.W., H.H. and P.-H.T. conducted the optical characterizations. Z. Zhou, N.S. and Z.F. performed the photocurrent measurements. H.F., M. Wang and Z. Liu conducted the ARPES characterizations. D.G., D.Z. and M. Wu contributed to the preparation of Cu(111) single crystals. Important contributions to the interpretation of the results and conception were made by K.L., C.L. and Z.-J.W. All the authors revised and commented on the paper.

Competing interests

The authors declare no competing interests.

Additional information

Supplementary information The online version contains supplementary material available at https://doi.org/10.1038/s41563-022-01361-8.

Correspondence and requests for materials should be addressed to Can Liu, Zhu-Jun Wang or Kaihui Liu.

Peer review information *Nature Materials* thanks Cheol-Joo Kim and the other, anonymous, reviewer(s) for their contribution to the peer review of this work.